NASA

Technical Memorandum 84937

Goddard X-Ray Astronomy Contributions to the IAU/COSPAR (1982)

November 1982

National Aeronautics and
Space Administration

Goddard Space Flight Center
Greenbelt, Maryland 20771

TABLE OF CONTENTS

EINSTEIN OBSERVATORY RESULTS ON ACTIVE GALACTIC NUCLEI*

R. F. Mushotzky and S. S. Holt

NASA/Goddard Space Flight Center, Greenbelt, MD 20771, U.S.A.

ABSTRACT

The Einstein Observatory, by virtue of its increased sensitivity and improved angular resolution, has increased substantially the number of known X-ray emitting active galactic nuclei. This has made possible the detailed study of the relation of X-ray flux to both the continuum flux in the optical and radio bands, and to the line emission properties of these objects. In addition, the Einstein imaging instruments have detected morphology in AGN X-ray emission, in particular from jetlike structures in Cen-A, M87, and 3C273.

The improved energy resolution and sensitivity of the spectrometers onboard the Observatory has provided detailed information on the geometry and ionization structure of the region responsible for the broad optical emission lines in a few AGN's. Such information, combined with detailed theoretical modeling and IUE and optical observations, have allowed us to construct a moderately detailed picture of the broad line region in these objects.

INTRODUCTION

The Einstein Observatory consisted of a focusing X-ray telescope with four focal plane (and one non-focal plane) instruments [1]. The two imaging focal plane instruments were the High Resolution Imager (HRI) with ~ 4" resolution and ~ 10 cm^2 sensitive area in roughly the .2-2 keV band, and the Imaging Proportional Counter (IPC) with ~ 60" resolution and 80 cm^2 sensitive area in the .2-3.5 keV band. The focal plane spectrometer with the most extensive results on active galaxies is the

*Review of literature finished April 1982

Solid State Spectrometer (SSS) which had a 6' diameter beam, 160 eV FWHM energy resolution, and ~ 100 cm^2 of effective area in the .5-4.0 keV band.

Because of the low background per spatial resolution element, made possible by the focusing optics, the Einstein Observatory had a threshold ~ 100 times lower than that of the HEAO-1 satellite for source detection by the imaging detectors and a threshold for detailed spectroscopy for sources at about the HEAO-1 limit. However, because most previous X-ray experiments were most sensitive in the 2-20 keV band, the overlap in energy band between Einstein and previous X-ray surveys is small.

During its lifetime, the Einstein Observatory looked at over 5000 targets of which ~ 1000 were active galaxies. In addition to the targets which were selected for observations, there were several hundred "serendipitous" observations of active galaxies that were in the ~ 1 square degree fields selected for other reasons.

SURVEYS

The main result of the Einstein observations of AGN, in our opinion, has been the confirmation of the ubiquity of X-ray emission from these objects; that is, X-ray emission is now established as a basic characteristic of AGN. This result, combined with the broad band HEAO-1 spectra, shows that much of the luminosity of the AGN often appears in the X-ray band. In fact, the several hundred active galaxies discovered because they were X-ray sources in Einstein imaging fields is a significant contribution to the total number of known AGN.

The vastly increased data base on X-ray luminosities from Einstein observations has enabled a number of optical, radio, and X-ray correlations to become well established. While several of these correlations were hinted at in pre-Einstein data [2,3] the large dispersions in the correlations require the larger HEAO-2 data base to confirm them.

A. X-ray and Optical Luminosities. In two large survey papers, Zamorani et al. (1981) [4] and Ku, Helfand, and Lucy (1980) [5] (KHL), it was shown that for optically selected AGN with $m_v < 18.5$ and $\log f_x > -12.2$ erg/cm^2 sec the optical and X-ray fluxes are strongly correlated. While there is a fair dispersion in the relation, the .5-3.5 keV X-ray luminosity L_x is typically ~ .2 of the optical

luminosity L_o for an AGN. The values range from upper limits of $L_x \lesssim 3x10^{-3}L_o$ to a maximum of $L_x \sim 3L_o$. Since the 3.5-60 keV luminosity of an AGN is usually 3.5 times its .5-3.5 keV luminosity, the typical intrinsic X-ray and optical luminosities are similar.

Recent work by Zamorani [6] and Reichert et al. [7] show that the X-ray to optical luminosity ratio decreases as a function of optical luminosity, with the higher luminosity objects having a lower X-ray to optical ratio such that $L_x \propto L_o^{.7}$. This relation appears to hold over roughly five orders of magnitude, between low luminosity AGN (Seyfert galaxies) at one end and QSO's at the other, and thus may argue for a continuity of properties between these objects. The L_x/L_o relation is an important constraint on theories of the energy generation mechanism in AGN's. Such theories must explain why QSO's have about an order of magnitude less X-ray emission per unit optical emission than Seyfert galaxies despite their strong spectral similarities.

B. X-Ray and Radio Properties. Many of the AGN in the initial surveys were radio loud objects, i.e., $L_R \gtrsim 2 \times 10^{-3} L_o$. Several authors have found that the X-ray to optical ratio is related to the radio flux such that radio bright quasars have about triple the average L_x to L_o ratio, with L_x/L_o also being a function of the radio to optical luminosity L_R/L_o. Using the objects in the KHL and Zamorani et al. surveys Setti and Woltjer [8] have shown that for optically bright AGN's ($L_o > 5 \times 10^{44}$ ergs/sec) L_x/L_o increases roughly linearly with L_R/L_o. F. Owen and co-workers [9,10] have shown that for objects selected on the basis of their strong high frequency radio flux, L_R/L_x shows a very small dispersion. Since the radio emission is due to synchrotron radiation from relativistic particles these correlations argue for a component of the X-ray radiation being due to emission from relativistic particles. These simple facts are complicated by the fact that the Setti-Woltjer relationship does not hold for low luminosity AGN's and that the Owen relation does not hold for a sample of optical or X-ray selected quasars. In addition, the variance in the Setti-Woltjer relation is quite large. We believe that this argues for a non-simple relationship between X-ray emission and relativistic particle population. KHL [5] argue that synchrotron radiation seems to be the dominant emission mechanism from the IR to X-ray for nearly all high luminosity AGN, with the radio bright objects having an additional X-ray emission component due to inverse Compton processes. Detailed X-ray spectra of BL Lac objects from the Einstein SSS

and HEAO-1 (a subset of radio bright AGN) tend to confirm the synchrotron origin of .2-4 keV X-rays from these objects. However, at present we do not have X-ray spectra of even a small sample of radio loud high luminosity AGN's.

C. X-Ray and Optical-UV Line Emission. It was noticed by Elvis et al. [2] based on the relatively small sample of AGN available in 1978, that some optical emission line properties are correlated with the X-ray luminosity. With the increased Einstein data base, several of these correlations are now well established. For example, Grindlay et al. [11], Kriss et al. [12], and Steiner [13] have shown that both the absolute Hβ luminosity and the OIII/Hβ ratio are well correlated with L_X for radio quiet objects. C. C. Wu and co-workers [14,15] have noted that the CIV luminosity is strongly correlated with the X-ray luminosity. Since these parameters are also well correlated with optical luminosity it is not surprising that they correlate with X-ray luminosity as well [7].

Detailed photoionization models of the broad line region in AGN have been able to qualitatively reproduce the correlation of the permitted lines with the optical and X-ray continuum levels. Because many of the low luminosity AGN have extremely similar X-ray and UV continua (Wu [15], Mushotzky [16]), it is possible to treat them as a homogenous group. However, it is not clear at present how to produce either the correlations of OIII/Hβ with L_X in FeII strong objects [13] or the lack of such correlation in FeII weak objects. Perhaps quantities other than the X-ray to optical ratio or the local spectral slopes are important, such as geometry or filling factor [17], or that selection effects are responsible for the apparent correlation.

The positive correlation of the infrared to soft X-ray ratio with the X-ray luminosity suggests that the IR continuum is influenced by the X-ray flux. Lawrence and Elvis [17] argue that there is a short wavelength non-thermal IR component that is directly correlated with the X-ray flux, and a long wavelength IR component due to dust heated by a source indirectly related to the X-ray emission.

Kriss et al. [12] have shown that there may exist a weak correlation of optical line width to X-ray flux; however, this depends mainly on including Seyfert II's in the sample. Since absorption by dust and gas can have a strong effect on the width of Hβ lines as well as on the Einstein fluxes (for it has been shown [16,17] that L_X

and N_H are anti-correlated), we consider this relation suspect, and it is most likely due to the fact that the broad wings of Hβ can be strongly reduced by reddening in the low luminosity objects. This observational selection effect probably also causes part of the OIII/Hβ versus L_X correlation since observed Hβ would be reduced in even slightly reddened objects. For $L_X > 5 \times 10^{43}$ erg/s, the roughly constant width of Hβ indicates that the mass motion of the line emitting gas is not directly related to the production of X-rays.

JETS

The X-ray emission from almost all active galaxies is not resolved by X-ray observations since the source of the radiation is probably smaller than a light year in size (3×10^{-3} arc sec at 20 Mpc), but deep exposures with the HRI and IPC have revealed X-ray emission from jets in Cen-A, 3C273, and M87 [18,19,20]. While the jets in M87 and 3C273 were well known before the Einstein observations, that in Cen-A was discovered in the X-ray band [22]. In all three cases the X-ray, optical, and radio jets have more or less the same structure [21], and the ratio of X-ray to optical fluxes is consistent with a synchrotron origin for the X-ray flux. However, this requires a steepening in the IR-optical region of the spectrum and thus indicates that the relativistic electron population of the jet likewise steepens at high energies. This is similar to the radio-optical-X-ray spectra of BL Lac objects and is consistent with the conjecture that BL Lac objects are jets seen end on [23].

The mere presence of jet related X-ray emission is strong evidence for reacceleration of particles in the jet with relativistic factors $\gtrsim 10^7$. The detailed structure of the jet in Cen-A [22] (the only one resolved by Einstein) independently argues for in situ acceleration (or reacceleration) since the size of knots ~ 10 arc sec (or ~ 250 pc in Cen-A) is so large that the X-ray emitting electrons could not live to cross the knot. The situation is even worse for relativistic electrons to cross from knot to knot or from the nucleus to the closest knot (a distance of ~ 750 pc). Evidence of hot gas in the central region of Cen-A [22] is roughly consistent with confinement of the jet by the thermal pressure of a hot ($T \sim 10^7$K) X-ray emitting plasma. Detailed X-ray spatial and spectral observations may give us information on the mechanisms of particle acceleration and transport and the mechanism of jet confinement.

Analysis of simultaneous IUE and SSS spectra of BL Lac objects show that, in at least three cases, the X-ray and UV spectral indices are similar and that extension of the UV spectrum can roughly predict the X-ray flux [23]. These data have been interpreted as a synchrotron emitting relativistic jet producing both the UV and X-ray radiation similar to the resolved jets of M87 and Cen-A.

"NEW" TYPES OF ACTIVE GALAXIES

Because of the ubiquity of X-ray emission from AGN, it is possible that "new" active galaxies can be discovered by their X-ray emission even though they may not show obvious optical or radio peculiarities. The optically "dull" galaxy NGC 4156 [24] may be such an object. Despite its proximity to the famous Seyfert NGC 4151, it was not discovered to have a active nucleus until Einstein's IPC and HRI observations showed a pointlike X-ray source of $L_X \sim 10^{42}$ ergs/sec which is ~ .1 of the X-ray luminosity of NGC 4151. This object has very weak optical emission lines and a "normal" continuum. This discovery shows the weakness of any individual survey method for AGN and the power of observing in a new frequency range in an unbiased manner. The "serendipitous" Einstein sources give us the opportunity to discover objects or properties of objects which we have not been clever enough to anticipate. In fact, the recent history of astronomy has been largely one of serendipitous discoveries (X-ray and radio pulsars, quasars, X-ray emission from clusters of galaxies, etc.)

The Einstein data on the very weak active nucleus in the "normal" galaxy M81 [25] corroborates the radio and optical data. The X-ray spectrum of M87 [26], in particular, requires a component in addition to the thermal gas which is indistinguishable in form from that of more luminous AGN (see below). This establishes a connection between QSO's and the nuclei of some "normal" galaxies over a range of 10^7 in luminosity for the active galaxy phenomena. It is of interest that the lowest luminosity AGN X-ray source is only ~ 10 times as luminous as the X-ray binary SMC X-1.

A serendipitous Einstein observation has revealed the first "narrow line" quasar. Stocke et al. [27] report that this X-ray source has a reddish continuum and relatively narrow 600 km/sec permitted lines. They argue that this object could be a prototype for a "new" class of "quasars" analogous to high luminosity Seyfert 2's.

It is clear from this very limited list that X-ray observations, whatever their biases, can find active nuclei in over a wide range of types and luminosities.

DETAILED SPECTRAL STUDIES

Because spectrometers are, in general, less sensitive than imaging experiments, the Einstein Observatory spectrometers were restricted to looking at the relatively high flux sources discovered by previous X-ray satellites. As reported by Holt [28] solid state spectrometer observations of active galaxies confirm that the $\alpha = 0.65$ energy index of the Seyfert I galaxies in the 2-60 keV band established by Mushotzky et al. [29] from HEAO-1 data extends down to 0.6 keV. Thus a universal power law form for AGN appears to hold over at least 2 decades in energy from 0.6 to 60 keV.

The most detailed results have been published on NGC 4151 [30]. The SSS data for this source do not show the form expected from a power law X-ray source extinguished by a uniform absorber: there is too much X-ray flux in the .5-2.0-keV band. The data can be well fit by a model in which the absorber is the broadline clouds, but their coverage is patchy so that X-rays can pass unextinguished through holes in the cloud cover. Since the ratio of 7.1 keV Fe absorption to 6.4 keV Fe fluorescent reemission suggests spherical symmetry in the absorbing material, the model fit to the data determine a mean covering factor of the clouds of ~ .9. This large covering factor is somewhat surprising in view of the .1 covering factor inferred from Lyman continuum measurements for high redshift quasars. In addition, determination of the energy of the Si, S, and Fe (from HEAO-1 data) K-edges demonstrate that the absorbing gas is cold.

This model essentially established the global geometry of the clouds, their approximate sizes, and their ionization state. It has also proven to be a key to understanding that the anti-correlation of X-ray absorption and luminosity in Seyferts discovered by HEAO-1, and possibly the anti-correlation of CIV equivalent width versus luminosity (the "Baldwin" effect) in high luminosity AGN's, are probably covering factor phenomena. The higher luminosity sources have, on the average, lower covering factors and, therefore, less X-ray absorption and weaker UV lines.

Detailed analysis of more SSS data is proceeding and at least one other low luminosity galaxy has a large covering factor. The upper limits on the column density for high luminosity sources from the SSS is consistent with the covering factor being inversely correlated with intrinsic luminosity. The SSS data do not exhibit X-ray emission lines from AGN; this lack of evidence for gas at temperatures between $10^{6.4}$ and $10^{7.8}$°K is consistent with recent models of the confining medium in the region emitting the broad optical emission lines.

THE COSMIC X-RAY BACKGROUND AND AGN

It was hoped that the vastly improved sensitivity of the Einstein Observatory would "solve" the "problem" of the Cosmic X-ray Background (CXB) either by resolving it into point sources or by establishing the contribution of different classes of objects to it.

Well before the launch of Einstein, it had been suggested [31] that AGN were most likely to be the dominant point source contributor to the CXB. From the initial Einstein survey of optically selected QSO's, it seemed, indeed, that an evolving population of AGN's (quasars) could easily make 100 percent of the ~ 1 keV CXB. In fact, as pointed out by Setti and Woltjer [32] and others, the CXB data seemed to require a turnover in the optical quasar counts at $m \sim 20$ in order that the CXB not be overproduced.

A variety of complications have conspired to prevent the unambiguous resolution of the CXB, however. First, the spectral data from HEAO-1 [33] have established that the CXB spectrum is much flatter ($\alpha \sim .4$) than those of Seyferts between a few keV and a few tens of keV; deZotti et al. [34] have shown that the sample of Seyfert galaxies from which we have data cannot be representative of the sample which might produce the XRB, even when redshifted to $z > 1$.

In addition, further work on quasar counts [35] and the radio-optical-X-ray correlations discussed in Section II showed that the problem has added complexity. While the last word is by no means in, the latest work [6,34,36,37] seems to indicate that the strongly evolving population of luminous ($M < -23.8$) quasars make up less than 45 percent of the CXB with most likely values nearer 20 percent (however different authors disagree somewhat such that the calculated contribution

of all AGN to the CXB could be from 60 to 10 percent). A point which is usually glossed over is that the Marshall et al CXB spectrum [33], consistent with a 45 keV bremsstrahlung spectrum, has the preponderance of the CXB energy density more than an order of magnitude higher in energy than the Einstein measurement. We might construct a scenario, therefore, whereby early AGN with spectra steeper than that typical of Seyferts might dominate the CXB near 1 keV and yet contribute virtually nothing to the total CXB energy density [38].

In order to truly resolve the problem one needs the spectra of AGN, particularly at energies > 10 keV, their luminosity function as a function of epoch, and better optical counts. Thus, despite the large increase in information on AGN provided by the Einstein Observatory, an unambiguous explanation for the CXB still remains a challenge

REFERENCES

1. R. Giacconi, et al. Ap. J. 230, 540 (1979).
2. M. Elvis, T. Maccacaro, A. Wilson, M. Ward, M. Penston, R. Fosbury, G. Perola, M.N.R.A.S. 183, 129 (1978).
3. A. Wilson, Proc. R. Soc. Lond. A. 366, 461 (1979).
4. G. Zamorani, et al. Ap. J. 245, 357 (1981).
5. W. H. Ku, D. J. Helfand, and L. B. Lucy, Nature, 288, 323 (1980).
6. G. Zamorani, in: Progress in Cosmology, Oxford International Symposium, 1982.
7. G. A. Reichert, K. A. Mason, J. R. Thorstensen, and S. Bowyer, Ap. J. submitted (1982).
8. G. Setti and L. Woltjer, Proceedings of the Vatican Study Week on Cosmology and Fundamental Physics, 1982.
9. F. N. Owen, D. J. Helfand, and S. R. Spangler, Ap. J. (Lett), 250, L55 (1981).
10. F. N. Owen and J. J. Puschell, A. J. 87, 595 (1982).
11. J. E. Grindlay, J. E. Steiner, W. R. Forman, C. R. Canizares, and J. E. McClintock, Ap. J. (Lett.), 239, L43 (1980).
12. G. A. Kriss, C. R. Canizares, and G. R. Ricker, Ap. J. 242, 492 (1980).
13. J. E. Steiner, Ap. J. 250, 469 (1981).
14. C. C. Wu, A. Boggess, T. R. Gull, R. F. Mushotzky, E. A. Boldt, S. S. Holt, and P. J. Serlemitsos, The First Year of IUE Symposium, 1979.
15. C. C. Wu, A. Boggess, and T. R. Gull, Ap. J. submitted (1982).
16. R. F. Mushotzky, Ap. J. 256, 92 (1982).
17. A. Lawrence, and M. Elvis, Ap. J., 256, 410 (1982).
18. E. J. Schreier, E. D. Feigelson, J. Delvaille, R. Giacconi, J. E. Grindlay, and A. C. Fabian, Ap. J. Lett, 234, L39 (1979).
19. E. J. Schreier, P. Gorenstein, and E. Feigelson, Ap. J. submitted (1982).
20. H. Tananbaum, X-Ray Astronomy, ed. R. Giacconi and G. Setti, 311, 1980.
21. E. Schreier, J. Burns, and E. Feigelson, Ap. J. in press (1982).
22. E. D. Feigelson, E. J. Schreier, J. P. Delvaille, R. Giaconni, J. E. Grindlay, and A. P. Lightman, Ap. J. 251, 523 (1981).
23. C. M. Urry, R. F. Mushotzky, Y. Kondo, K. R. M. Hackney, and R. Hackney, Ap. J. in press (1982).
24. M. Elvis, E. J. Schreier, J. Tonry, M. Davis, and J. Huchra, Ap. J. 246, 20 (1981).
25. M. Elvis, and L. Speybroeck, Ap. J. in press (1982).

26. S. Lea, R. F. Mushotzky, and S. S. Holt, Ap. J. in press (1982).
27. J. Stocke, J. Liebert, T. Maccacaro, R. E. Griffiths, and J. E. Steiner, Ap. J. 252, 69 (1982).
28. S. S. Holt, X-Ray Astronomy from the Einstein Observatory, ed. R. Giaconni, 173, 1981.
29. R. F. Mushotzky, F. E. Marshall, E. A. Boldt, S. S. Holt, and P. J. Serlemitsos, Ap. J. 235, 377 (1980).
30. S. S. Holt, R. F. Mushotzky, R. H. Becker, E. A. Boldt, P. J. Serlemitsos, A. E. Szymkowiak, and N. E. White, Ap. J. (Letters), 241, L13 (1980).
31. G. Setti, and L. Woltjer, Astrophys. Sp. Sci. 9, 185 (1970).
32. G. Setti, and L. Woltjer, Astron Astrophys. 76 L1 (1979).
33. F. E. Marshall, E. A. Boldt, S. S. Holt, R. B. Miller, R. F. Mushotzky, L. A. Rose, R. E. Rothschild, and P. J. Serlemitsos, Ap. J. 235, 4 (1980).
34. G. DeZotti, E. A. Boldt, A. Cavaliere, L. Danese, A. Franceschini, F. E. Marshall, J. Swank, and A. Szymkowiak, Ap. J. 253, 47 (1982).
35. D. Koo and R. Kron, Astron. Astrophys 105, 107, (1982).
36. A. K. Kembhavi, and A. C. Fabian, M.N.R.A.S. 198, 921 (1982).
37. A. Cavaliere, L. Danese, G. DeZotti, A. Franceschini, 15th ESLAB Symposium on X-Ray Astronomy, 1981.
38. S. S. Holt, X-Ray Astronomy, ed. R. Giacconi and G. Setti, 327, 1980.

X-RAY SPECTRA OF YOUNG SUPERNOVA REMNANTS

S.S. Holt
Laboratory for High Energy Astrophysics
NASA/Goddard Space Flight Center
Greenbelt, Maryland 20771

A. HISTORICAL NOTES

The early identification of the strong X-ray source in Taurus with the Crab nebula (Bowyer et al. 1964) was the first milestone in the association of X-ray emission with supernova remnants. Unfortunately, it proved to be "red herring" which clouded the interpretation of X-ray emission from supernova remnants for a decade. Because the Crab was one of the brightest X-ray sources in the sky at a few keV, the interrogation energy of the early surveys, and because it was the first (and for several years the only) X-ray source conclusively identified, the potential association of a supernova origin with the large body of unidentified X-ray sources was not an unreasonable hypothesis.

By 1970 proportional counter spectra from rocket-borne observations, with resolving power $E/\Delta E < 2$, were available for Cas A and Tycho as well as the Crab (Gorenstein, Kellogg and Gursky 1970). Since the statistical significance of the data points were exposure-limited, they were fittable with either bremsstrahlung continua with temperatures of $\sim 10^7$ K or power-law spectra; the analogy with the Crab suggested to many interpreters of the data that the latter representations of the spectra were more appropriate. By that time the Crab spectrum was well-measured to be a power-law with $\alpha \sim 1$ between 1-100 keV, and relatively well-understood (from the point of view of available energy, if not energy transfer) as arising from the non-thermal conversion of rotational energy from its pulsar. Similar pulsars which were unobservable because of their beaming characteristics were suggested for other young supernova remnants, since only young pulsars could provide the required rotational energy loss (e.g. Pacini 1971). Similarly, models featuring hidden pulsars in sources not associated with traditional supernova remnants (e.g. Davidson, Pacini and Salpeter 1971) were relatively popular.

The discovery of "X-ray pulsars" (Giacconi et al. 1971), distinguishable from radio pulsars like the Crab by their inability to account for the source luminosity from rotational energy loss, provided the key to understanding the energy generation mechanism of the non-SNR

sources in terms of mass accretion onto neutron star components of binary systems, as had been suggested by Shklovsky (1967). But what about the young SNRs Cas A and Tycho? An early suggestion by Heiles (1964), that the SN blast wave sweeping up the interstellar medium into a shell of shocked material would provide an observable X-ray source, seemed more appropriate to older remnants in which enough mass had been swept up to provide an adequate emission measure, and enough time had elapsed to allow the radiating shell to equilibrate at a temperature low enough to cool efficiently (e.g. Woltjer 1972). Nevertheless, a blast wave interpretation for the young SNRs increased in popularity as the newer data indicated better agreement with a thermal spectrum. The key experimental result was the discovery of Fe line emission from Cas A (Serlemitsos et al. 1973) which, although originally interpreted by its discoverers as arising from charge exchange with ~ 10 MeV/nucleon cosmic rays, was quickly recognized as the signature of thermal processes in the remnant. As data from satellite experiments became available (Charles et al. 1975; Pravdo et al. 1976; Davison, Culhane and Mitchell 1976) this picture was refined to require two separate thermal components for consistency with these higher statistical precision data. Itoh (1977) suggested that the harder of these two components was associated with the blast wave, while the softer was associated with a thin, dense shell of ejecta accumulated from the "reverse shock" postulated by McKee (1974). The history of Cas A and Tycho measurements in the decade preceding the first spectral data from Einstein is given in Table 1.

Table 1

EARLY THERMAL FITS TO CAS A AND TYCHO

	Cas A		Tycho	
Ref	Tlow	Thigh	Tlow	Thigh
Gorenstein et al. 1970	----	1.25± .34	----	2.2±1.0
*Brisken 1973	.83±.06	----	.45±.05	----
Hill et al. 1975	----	2.3	----	1.9
Charles et al. 1975	.73±.20	2.6 ±1.0	----	----
Pravdo et al. 1976	< .7	3.9 ± .6	----	----
Davison et al. 1976	1.08±.03	5.2 ± .6	.55±.04	3.5± .3

*refined analysis of data of Serlemitsos et al. (1973)

B. THE EINSTEIN SSS DATA

The newer Einstein data summarized here are from the Solid State Spectrometer (SSS), a cryogenically-cooled Si(Li) device with a FWHM energy resolution of ~ 160 eV over its effective 0.5-4.5 keV energy range (see Holt et al. 1979 for experiment details). The spectra I shall discuss have already been preliminarily reported in the literature. The new information presented here will be of two kinds: a

refined set of experimental spectra with all sources of background over the full 0.5-4.5 keV band now properly accommodated, and some remarks about the progress which has been made in the physical modelling of SNR to reproduce these spectra.

A Crab spectrum is presented in Figure 1; it represents one of ~ 100 such spectra obtained over the lifetime of the experiment, all of which were used for calibration purposes to ensure uniformity in the interpretation of detector response with time. The input spectrum is presumed to be a featureless power law of index $\alpha = 1.1$ observed through an interstellar medium of cosmic abundance with column density $N_H = 3 \times 10^{21}$ atoms cm^{-2}. Note that the experiment introduces an apparent kink in the spectrum at ~ 0.8 keV (arising from the nickel with which the telescope is coated), but that any other features (particularly ones assocaited with silicon, of which the detector is made, and which might be expected near 1.8 keV) are much smaller than the statistical precision of one of the displayed pulse-height channels in a typical measurement. The Crab spectrum is illustrative, therefore, of the fact that any potential line features in the spectra are not systematically induced in the detector.

The line features which are observed in young SNR spectra are indicated in Figure 2, where are plotted the pulse height data from an exposure to the Tycho (SN 1572) remnant, together with a comparison spectrum for illustrative purposes. The comparison spectrum is that expected from a T = 0.5 keV solar-abundance plasma in thermal equilibrium, viewed through an interstellar column density of 2×10^{21} atoms cm^{-2}; this comparison histogram is not convolved through the detector response, but is smeared to a FWHM resolution of ~ 50 eV with exactly the same bin widths as the experimental data. The shaded portion of the comparison spectra is the contribution from Fe-L emission from the isothermal plasma, and the darkened portion the contribution from Si-K emission; the four blackened bumps represent Si^{+12} Kα, Si^{+13} Kα, Si^{+12} Kβ and Si^{+12}Kγ in order of increasing energy. From the obvious line identifications, therefore, it is clear that the observed lines are characteristic of a relatively low temperature (e.g. T = 0.5 keV) plasma, in the sense that the helium-like lines of the Z > 10 constituents are evident while the hydrogen-like lines are not, but the equivalent continuum widths of the observed lines are considerably in excess of the equilibrium values for solar abundances. Most of the remainder of this paper will be devoted to a discussion of the modelling of such spectra.

C. SPECTRAL MODELLING

Figure 1 displays the SSS spectrum from Cas A. As originally reported by Becker et al. (1979), the data cannot be fitted with a single equilibrium temperature with any abundance distribution; instead, it can be reasonably well-fitted with two equilibrium components. The lines are consistent with an equilibrium plasma at T ≈ 0.65 keV (albeit

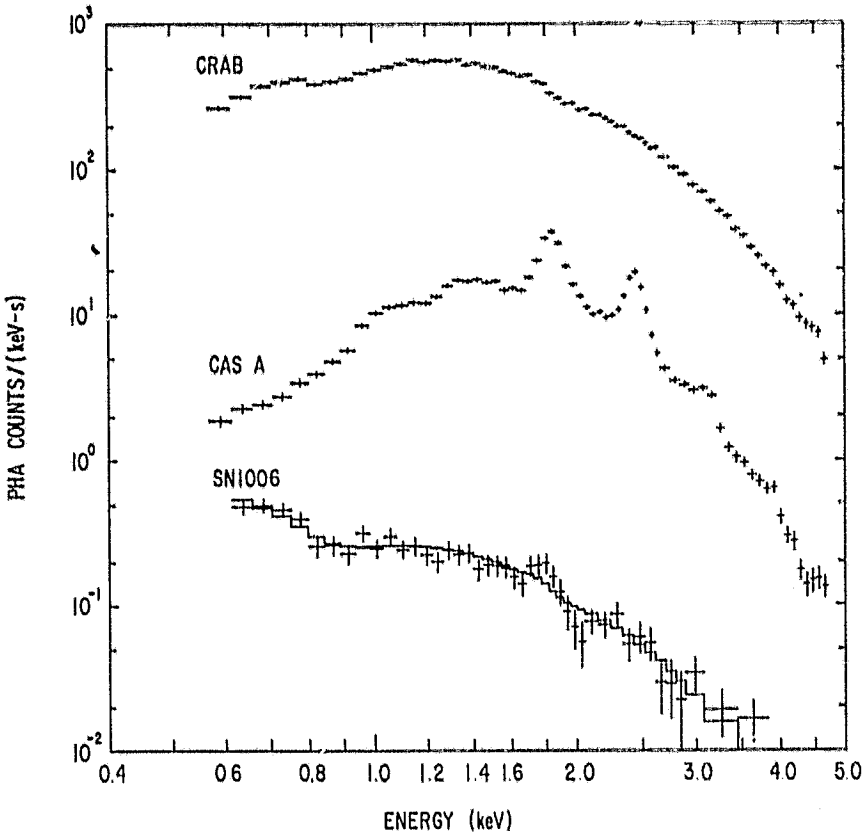

Figure 1. Experimental SSS spectra for the Crab nebula, CasA and SN1006. The solid histogram through the SN1006 data points represents a power law of index $\alpha = 1.2$ observed through a column density of 9×10^{20} atoms cm^{-2}.

with overabundances in the line-emitting components), but a higher temperature component is required to replicate the harder continuum observed and to smoothly connect to the higher energy measurements; because the bremsstrahlung continua from any temperatures $\gtrsim 3$ keV are indistinguishable in the SSS 0.5-4.5 keV bandpass, a fixed 4 keV was chosen to approximately connect to the higher energy measurements.

The data presented in Figure 1 are somewhat more refined than originally presented in Becker et al. (1979), but the important source-fitting parameters are not substantially changed. In particular, the best-fit low temperature component (for a 2-temperature equilibrium fit) is still $T \simeq .65$ keV, and the Si abundance is ~ 1.5 times solar, as determined from the simultaneous fitting of the lines and the continuum. Relative to this inferred Si abundance, the inferred abundances of other important constituents relative to solar proportions are S/Si(~2), Ar/Si(~4), Ca/Si(~2) and Mg/Si(~.1). The only significant difference between the results of the present modelling and that originally reported is in the Fe abundance, as the model extension to

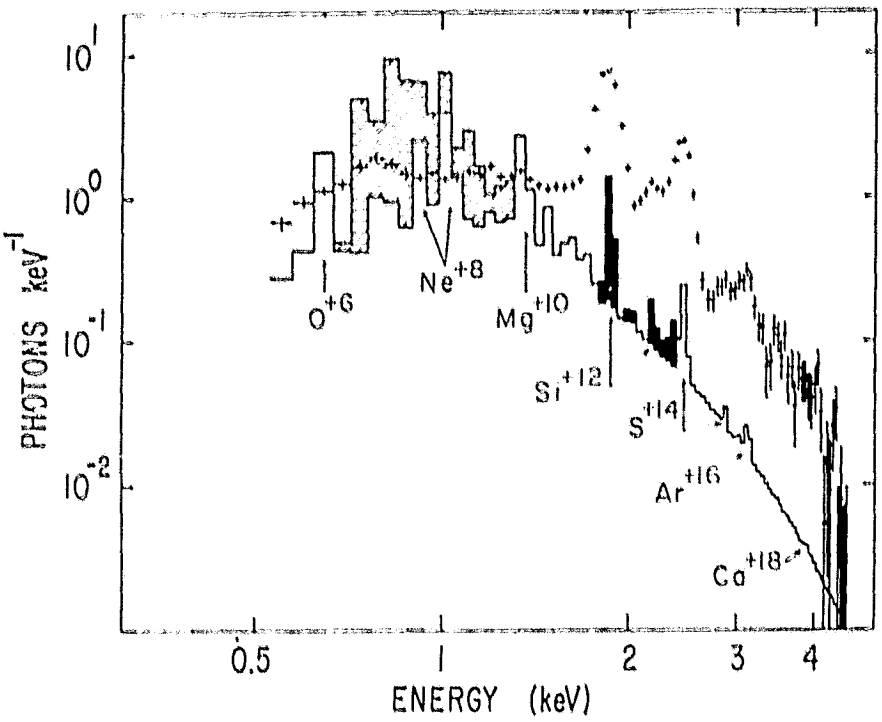

Figure 2. Experimental SSS spectrum of the Tycho SNR, compared with the expected spectrum from a solar-abundance equilibrium plasma at T = 0.5 keV as it would be observed with a detection system which has an energy-independent response (see text for additional details).

lower energies changes what was previously a measured Fe/Si ~ .5, relative to solar, to an upper limit. The lack of a pronounced increase with Z in the relative overabundances of Si, S, Ar and Ca suggests that the standard qualifications regarding non-equilibrium ionization may obscure the important qualitative conclusions that may be drawn from the spectrum. If, as suggested by Fabian et al. (1980) from an interpretation of the X-ray morphology, the remnant is in the free expansion phase and the low energy X-ray emission is dominated by the ejecta, the clumpiness of the emission suggests a situation closer to equilibrium (at least within the clumps) than would a smoother distribution, as the Rayleigh-Taylor-induced density enhancements should equilibrate more rapidly than would the unclumped ejecta (see Chevalier 1982 for a discussion of the unclumped density distribution which might be expected from a system like Cas A with pre-SN mass loss). The modest abundance enhancement of Si-group material implied by the equilibrium simplification may, therefore, better characterize the spectrum than would a detailed (non-unique) calculation, at least until such time as measurements with better spectral and spatial resolution are available.

In contrast to Cas A, the three Type I remnants Tycho, Kepler and SN1006 display a clear necessity for non-equilibrium effects. The spectra of Tycho and Kepler bear marked similarities to each other (see

Figure 3); utilizing the same two-temperature equilibrium model as a starting point, both have low temperatures of T ≈ .5 keV. Tycho requires a Si abundance which is approximately an order of magnitude in excess of solar (Kepler requires about half the Tycho Si abundance), and for both remnants the allowable relative abundances of S, Ar and Ca increase with atomic number (in the newer equilibrium fits, these implied abundances are even higher than those in Becker et al. 1980a and Becker et al. 1980b), in accordance with the expectation for a non-equilibrium plasma which is still ionizing. The application of a Sedov approximation (Shull 1983; Hamilton, Sarazin and Chevalier 1983)

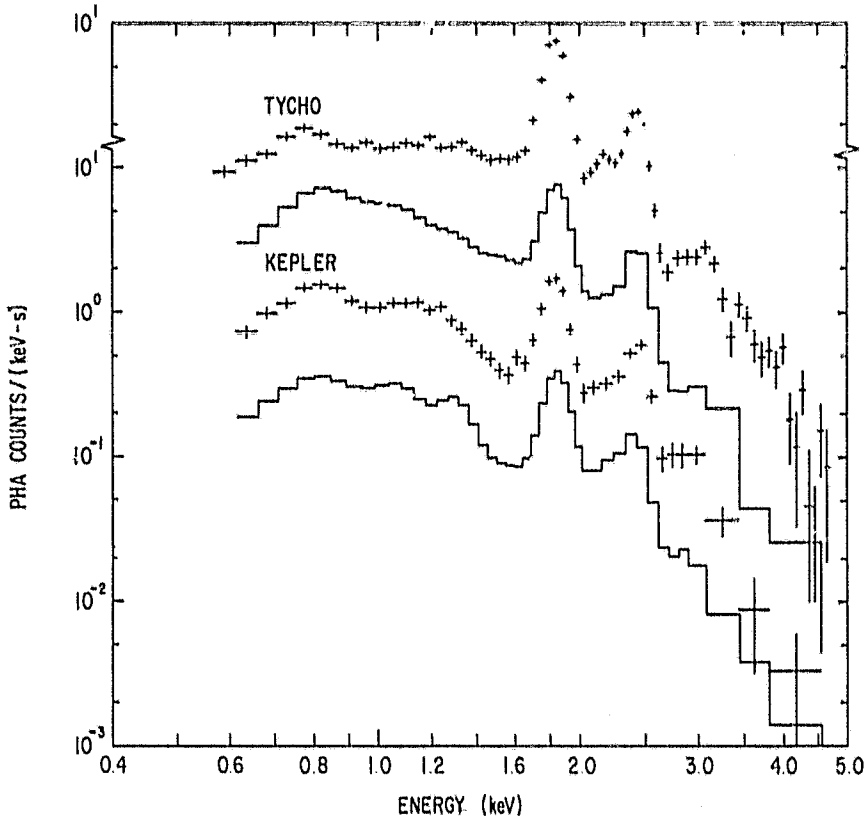

Figure 3 - Experimental SSS spectra of the Tycho and Kepler SNRs. The solid histograms, arbitrarily placed above and below the Kepler spectrum, represent different fits to Kepler of comparable statistical adequacy. The upper fit is a two-temperature equilibrium model for which the abundances are free parameters (see text), while the lower fit is a Sedov model with similarly unconstrained abundances; many such models (with differing n_e electron fitted with comparable statistical adequacy, but all require S_i overabundances relative to solar.

relieves this latter problem, but its applicability may be problematic. A variety of Sedov models with and without clumping (and with and without the assumption of rapid equilibration of the electrons with the shock) all yield pronounced overabundances of Si, comparable to those found in the equilibrium fits. The relative abundance ratios for the higher-Z constituents (i.e. those which are identifyable by their K-emission) are no longer unreasonably high, however; S/Si is still ~ 2 (as it appears to be for all SNR fits), but Ar/Si and Ca/Si need not be much higher than unity (i.e. solar). The utilization of a Sedov model (properly constrained to the observable luminosity at the best-estimated distance, with reasonable values of $\eta = E_o n_o^2$) is questionable a priori if the interpretation of the X-ray morphology given by Seward, Gorenstein and Tucker (1983) is correct, i.e. if the large fraction of the X-ray luminosity arises from clumped reverse-shocked ejecta rather than from the blast wave. Interestingly, Hamilton (this volume) has demonstrated that the emission from the ejecta can be modelled with a Sedov approximation (where the parameter η is a bit more obscure), allowing fits which better match the data in detail (Sarazin, Hamilton and Chevalier, this volume).

A continuing feature of all the fits is the lack of marked overabundances of Fe, as might be inferred from its L-emission (see Figure 2) in accordance with current models of Type I SN which release a large fraction of a solar mass of Fe-group material. The primary difference between the Tycho and Kepler spectra of Figure 3 is in the Fe L-emission; Fe is virtually undetectable from Tycho, but is required at about the level Fe/Si ~ 1 (relative to solar) in the various equilibrium and non-equilibrium Kepler fits. Even in Kepler, this abundance is at least an order of magnitude below that expected if the Fe-group material is well-mixed into the X-ray-emitting plasma. Clearly, the retention of the Fe-rich model requires the not-unreasonable assumption that the heavier ejecta is interior to the Si-group ejecta, and has not yet been significantly reverse-shocked.

The X-ray spectrum of SN1006 is even more puzzling. Unlike the younger Type I remnants discussed above, there is no statistically significant evidence for K-line emission. In fact, the X-ray spectrum can be fit with a Crab-like power law ($\alpha \sim 1$) from 0.5 keV out to at least 20 keV (Becker et al. 1980c). It is worth noting that the higher energy X-ray spectra of other SNR can be relatively well-fit by power law approximations, but with spectral indices which are much larger (i.e. the younger and more initially energetic SNR Cas A can be fit with $\alpha \sim 3$, while Tycho can be fit with $\alpha \sim 4$; see Figures 1 and 2 of Pravdo and Smith 1979). Fabian, Stewart and Brinkmann (1982) have suggested that the appearance of a featureless power law may arise from the superposition of emission from differing thermal shells. If the intermediate-Z metals are substantially locked in grains, and if the reverse-shock has long-since passed through the Fe-rich ejecta (so that the remnant interior has cooled to $\sim 10^6$ K), the absence of the prominent lines observed in the younger remnants may be reconciled. It should be noted, however, that the spectral hardness of the high energy continuum may be more easily explained with non-thermal processes, e.g.

synchrotron radiation from electrons accelerated near the blast wave (Reynolds and Chevalier 1981) or possibly even from the naive picture of a hidden pulsar which was so popular ten years ago.

D. FINAL REMARKS

The combination of higher-energy (> 5 keV) spectral data from pre-Einstein investigations (see Pravdo, this volume) with morphological and spectral data from all the Einstein instrumentation provides a powerful tool for studying SNRs. This evidence is not totally conclusive in all particulars, however. The modelling of the SSS data requires a complete time-dependent coupled solution of the hydrodynamics and ionization, including whatever density inhomogeneities may exist in each specific remnant, since the experiment aperture is 6 min in diameter. Better spectral resolution than its 160 eV FWHM would be useful (insofar as K-emission contributions from differing multiplet components would then be resolvable), but the present resolution is sufficient to distinguish H-like and He-like ionization states. Much more important would be the application of the available spectral resolution to much more localized regions of the SNR, so that differential information would not have to be extracted from the attempted separation into components of the whole-remnant spectrum.

The available procedure is necessarily non-unique, and cannot unambiguously distinguish whether the electrons in the recently shocked plasma can quickly equilibrate with the heavier constituents (as it least some fraction must, from > 10 keV measurements; Pravdo and Smith 1979) or whether they require a Coulomb equilibration timescale (typically longer than the remnant age) to do so; the two cases yield very different bremsstrahlung continua and, hence, can result in very different blast/ejecta proportions and abundances. Unfortunately, fits to the whole remnant data with either assumption for the electron equilibration timescale can yield results of comparable statistical significance. With no independent reason for fixing such otherwise indeterminate parameters, therefore, model uniqueness is not assured. Until such time as more independent information exists (e.g. from the application of like quality spectral data with much finer spatial resolution, so that some separability of otherwise degenerate fitting parameters can be obtained), a satisfactory fit to the whole-remnant spectral data cannot guarantee a unique detailed explanation.

My thanks to the many members and associates of the GSFC X-ray group, past and present, who have contributed to our ongoing program of research. Andrew Szymkowiak, in particular, is responsible for the large fraction of the previously unpublished work on which much of this discussion is based.

REFERENCES

Becker, R.H., Holt, S.S., Smith, B.W., White, N.E., Boldt, E.A., Mushotzky, R.F., and Serlemitsos, P.J. 1979, Ap. J. (Letters) 234, L73.

Becker, R.H., Holt, S.S., Smith, B.W., White, N.E., Boldt, E.A., Mushotzky, R.F., and Serlemitsos, P.J. 1980a, Ap. J. (Letters) 235, L5.
Becker, R.H., Boldt, E.A., Holt, S.S., Serlemitsos, P.J., and White, N.E. 1980b, Ap. J. (Letters) 237, L77.
Becker, R.H, Szymkowiak, A.E., Boldt, E.A., Holt, S.S., and Serlemitsos, P.J. 1980c, Ap. J. (Letters) 240, L33.
Bowyer, C.S., Byram, E.T., Chubb, T.A., and Friedman, H. 1964, Science 146, 912.
Brisken, A.F. 1973, PH.D. Thesis (University of Maryland).
Charles, P.A., Culhane, J.L., Zarnecki, J.C., and Fabian, A.C. 1975, Ap. J. (Letters) 197, L61.
Chevalier, R.A. 1982, Ap. J. 258, 790.
Davidson, K., Pacini, F. and Salpeter, E.E. 1971, Ap. J. 168, 45.
Davison, P.J.N., Culhane, J.L., and Mitchell, R.J. 1976, Ap. J. (Letters) 206, L37.
Fabian, A.C., Stewart, G.C., and Brinkmann, W. 1982, Nature 295, 508.
Fabian, A.C., Willingale, R., Pye, J.P., Murray, S.S., and Fabbiano, G. 1980, Mon. Not. R. Astron. Soc. 193, 175.
Gorenstein, P., Kellogg, E.M., and Gursky, H. 1970, Ap. J. 160, 199.
Hamilton, A.J.S. 1983, this volume.
Hamilton, A.J.S., Sarazin, C.L., and Chevalier, R.A. 1983, Ap. J. Suppl., in the press.
Heiles, C. 1964, Ap. J. 140, 470.
Hill, R.W., Burginyon, G.A., and Seward, F.D. 1975, Ap. J. 200, 158.
Holt, S.S., White, N.E., Becker, R.H., Boldt, E.A., Mushotzky, R.F., Serlemitsos, P.J., and Smith, B.W. 1979, Ap. J. (Letters) 234, L65.
Itoh, H. 1977, Publ. Astron. Soc. Japan 29, 813.
Pacini, F. 1971, Ap. J. (Letters) 163, L17.
Pravdo, S.H., Becker, R.H., Boldt, E.A., Holt, S.S., Rothschild, R.E., Serlemitsos, P.J., and Swank, J.H. 1976, Ap. J. (Letters) 206, L41.
Pravdo, S.H. and Smith, B.W. 1979, Ap. J. (Letters) 234, L195.
Pravdo, S.H. 1983, this volume.
Reynolds, S.P. and Chavalier, R.A. 1981, Ap. J. 245, 912.
Sarazin, C.L., Hamilton, A.J.S., and Chevalier, R.A. 1983, this volume.
Serlemitsos, P.J., Boldt, E.A., Holt, S.S., Ramaty, R., and Brisken, A.F. 1973, Ap. J. (Letters) 184, 1.
Seward, F., Gorenstein, P., and Tucker, W. 1983
Shklovsky, I.S. 1967, Ap. J. (Letters) 148, L1.
Shull, J.M. 1982, Ap. J. (Letters), in the press.
Woltjer, L. 1972, Ann. Rev. Astron. Ap. 10, 129.

Kirshner: The principal optical result on Cas A is that oxygen is greatly enhanced. The SSS spectra only give the ratio of Si, S and the rest to oxygen. Are the X-ray data consistent with the extraordinary abundances seen in the optical filaments?

Holt: Because the energy resolution of the SSS does not allow us to completely separate line and continuum contributions to the experimental spectrum, and because the bremsstrahlung continuum is dominatted by oxygen (if present in at least solar proportions to hydrogen), it is not possible to define a totally unambiguous reference for the

"abundances"--even before addressing the problem of how appropriate an equilibrium model should be for the whole-remnant specrum of Cas A. If we assume that the portion of the spectrum below ~ 3 keV is dominated by the ejecta in the fast-moving knots, the implied Si/O ratio is well within a factor of two of the values given in Table 5 of Chevalier and Kirschner (1978).

Tuffs: Is a shock velocity of, say, 2800 km s^{-1} for Cas A consistent with the observed line ratios?

Holt: The shock temperature defined by the shock velocity (for a Sedov solution) is > 10^8 K, or much too high to match the observed line ratios. The experimental preponderance of helium-like to hydrogen-like lines forces the equilibrium fits to the spectra of Tycho and Kepler, in addition to that of Cas A, to contain a component at < 10^7 K which dominates below ~ 3 keV. At higher energies, however, there is continuum evidence for plasma approaching equilibrium with the blast wave (Pravdo and Smith 1979).

Chevalier: With regard to the non-uniqueness of the X-ray spectral fits, do all the models have the proper ages, radii and X-ray luminosities?

Holt: The Sedov models we have attempted to fit to Tycho and Kepler, such as that displayed in Figure 3 for Kepler, are those for which the ages are correct and the radii/luminosities are consistent with reasonable distance estimates. We don't take seriously any fortuitous spectral fits with unreasonable model implications.

Fedorenko: Are the power-law X-ray spectra consistent with the equilibrium particle distribution functions? What is the mechanism of radiation?

Holt: I presume that you are referring to the spectrum of SN1006, for which we find that a power-law is an adequate fit to our data. It is certainly possible to synthesize power-law fits from combinations of equilibrium particle distribution functions (see the early attempt by Sartori and Morrison 1967 to so reproduce the spectrum of the Crab), but the consistency of the same power law over two orders of magnitude in energy is suggestive of a synchrotron origin for the X-ray emission.

Fabian: Since the electron-ion equilibration time is often greater than the age of the remnant, how do you know what high energy spectral form should be fit to the continuum data (e.g. in SN1006)?

Holt: In the case of Sedov models, we utilize computer-generated differential spectra instead of limiting analytic forms, which are dependent upon the usual model parameters (including time) as well as upon physical assumptions such whether electron-ion equilibration can be more rapid than specified by Coulomb interactions alone. Although a power-law appearance is certainly possible for the superposition of

non-equilibrium as well as equilibrium thermal spectra, the extension of the form to at least 20 keV for SN1006 argues against it because such a hard spectrum ($\alpha \sim 1$) suggests a blast wave with much higher velocity than that of the younger and more energetic Cas A, for example (with $\alpha \sim 3$); the appearance of any photons at all at 20 keV requires a current blast wave velocity of 4000 km s^{-1}, but the maintainance of the hard spectral form requires that the blast wave velocity is considerably larger than that. The assumption of a slow equilibration time only exacerbates the problem, as it is then even more difficult to produce X-rays with energies comparable to the value for equilibrium with the blast wave and, hence, more difficult to produce both a hard spectrum and its extension out to 20 keV.

HIGH RESOLUTION X-RAY IMAGES OF PUPPIS A AND IC 443

R. Petre[1], C.R. Canizares[2], P.F. Winkler[3], F.D. Seward[4], R. Willingale[5], D. Rolf[5], and N. Woods[5]

[1]NAS/NRC Research Associate at Laboratory for High Energy Astrophysics, NASA/GSFC
[2]Center for Space Research, MIT; Alfred P. Sloan Foundation Fellow
[3]Middlebury College
[4]Harvard/Smithsonian Center for Astrophysics
[5]Leicester University

ABSTRACT

We present soft X-ray photomosaic images of two supernova remnants, Puppis A and IC 443, constructed from a series of exposures by the Einstein imaging instruments. The complex morphologies displayed in these images reflect the interaction between "middle-aged" supernova remnants and various components of the interstellar medium. Surface brightness variations across Puppis A suggest that inhomogeneities on scales from 0.2 to 30 pc are present in the interstellar medium, while the structure of IC 443 is apparently dominated by the interaction between the remnant and a giant molecular cloud.

In supernova remnants that have evolved well into their adiabatic expansion phase ($t \sim 10^4$ yr), the bulk of the soft X-ray emission arises from recently shock-heated interstellar matter. The soft X-ray morphology of such "middle-aged" remnants will be influenced by any large or small scale inhomogeneities in the interstellar medium (ISM) they encounter. Consequently, these supernova remnants serve as excellent remote probes of the structure of the ISM.

We present and briefly discuss here high-resolution soft X-ray images of two such "middle-aged" remnants, Puppis A and IC 443. Despite their similarity in age ($\sim 10^4$ yr), distance ($\sim$ 2 kpc) and diameter (25-30 pc), these two remnants display markedly different morphologies, presumably due largely to their different environments. A more extensive discussion of Puppis A may be found in Petre et al. (1982a); the IC 443 imaging results, along with spectral studies using the

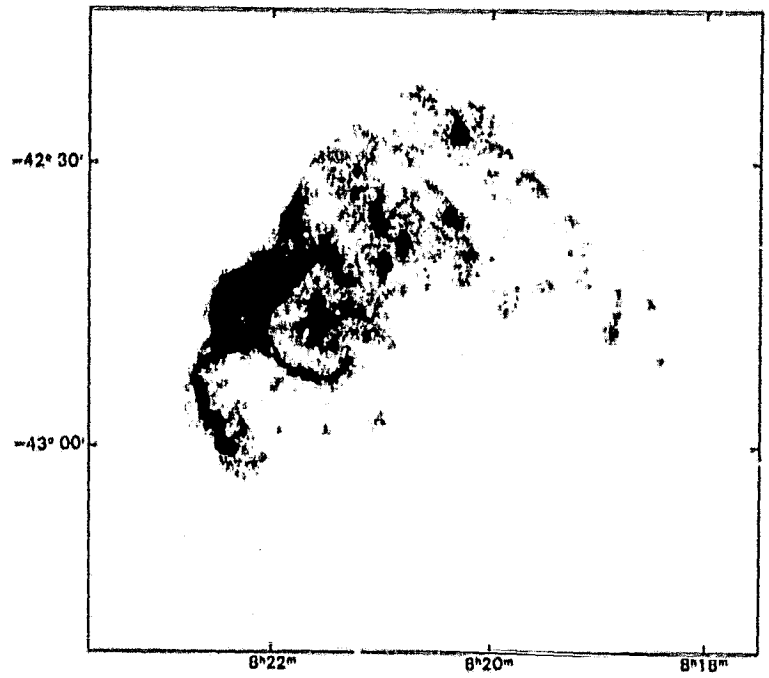

Figure 1: A high-resolution 0.1-4 keV photomosaic map of Puppis A.

Einstein Solid State Spectrometer (SSS) and the HEAO 1 A-2 MED, will appear in Petre et al. (1982b).

Puppis A

Figure 1 shows a high-resolution X-ray image of Puppis A in the energy range 0.1-4.0 keV. The map is an exposure-corrected photomosaic of 11 Einstein High Resolution Imager (HRI) exposures, binned in 8" pixels. The image reveals an ISM with structure on many scales. First, there is a general decrease in X-ray surface brightness, by a factor of at least 20, from northeast to southwest across the remnant, perpendicular to the galactic plane. This effect is probably due to a local density gradient in the ISM of at least a factor of 4 over a scale of ~ 30 pc. Second, the surface brightness variations in the interior and along the shell suggest a preshock ISM containing many small density variations (factors of 2), about an average of ~ 1 cm^{-3}, over scales from 0.2 to 10 pc. Despite the surface brightness variations along the shell, the pronounced limb-brightening profiles are for the most part consistent with that expected for an adiabatically expanding blast wave, suggesting that the local clumpiness of the interstellar matter does not prevent the adiabatic model from being locally valid. Finally, in addition to the filamentary structure representing small density perturbations, Puppis A contains two bright knots of emission along the shell, one in the east and one in the northwest. These knots are probably shocked interstellar clouds with preshock density of 10-20 cm^{-3} and diameter 1-2 pc.

IC 443

Figure 2 depicts a 0.2-3.1 keV map of IC 443, overlayed on a Palomar Sky Survey red plate. The map is an exposure-corrected, Wiener-filtered photomosaic of three Imaging Proportional Counter (IPC) images,

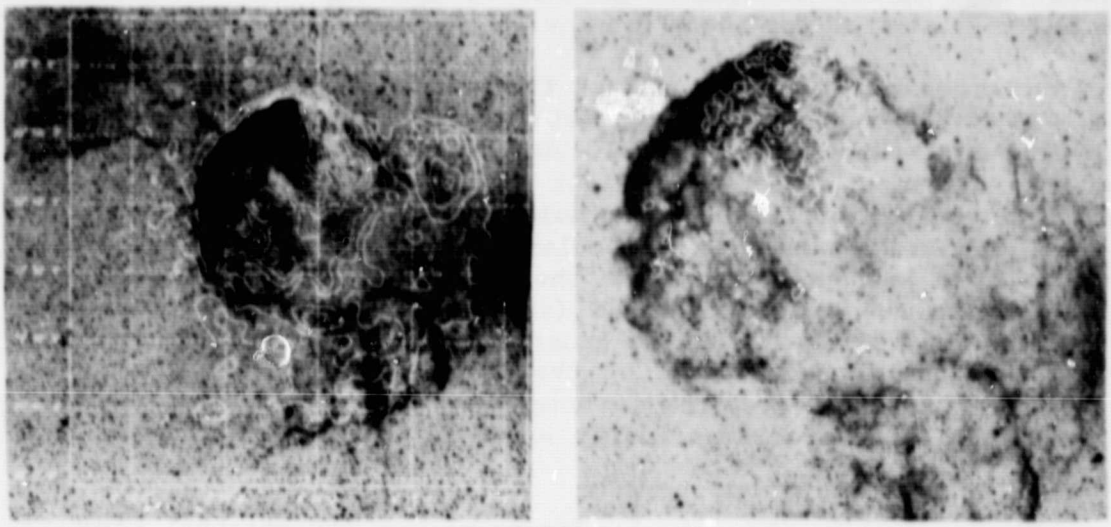

Figure 2 (left): A 0.2-3.1 keV image of IC 443, superposed on a Palomar Sky Survey red plate. This map is a photomosaic of three IPC images. Figure 3 (right): An HRI photomosaic of IC 443, superposed on the Palomar red plate.

binned in 32" pixels. The contours scale linearly with surface brightness. Although X-ray emission is detected from the entire SNR, the remnant does not appear to be limb-brightened. The average surface brightness in the vicinity of the bright northeastern optical filaments is a factor of ~ 4 higher than elsewhere. This network of filaments has apparently been created by the collision of the shock front with a giant molecular cloud, which is observed in CO to extend well beyond IC 443 to the northeast (Scoville et al. 1977; Cornett, Chin and Knapp 1977).

A sharper view of the northern portion of IC 443 is shown in Figure 3. This map is an exposure-corrected, Wiener-filtered photomosaic of three HRI images, with 16" binning, whose coverage of IC 443 is represented approximately by the area over which the grid appears. The contour levels were chosen to reveal the highest X-ray surface brightness features; X-rays were actually detected by the HRI from everywhere in the complex of optical filaments, with the notable exception of the finger of optical extinction extending northeastward into the filaments.

The HRI map emphasises the dominant X-ray feature, a ~ 15′ diameter region which partially overlaps the optical filaments. The

pressure of the X-ray emitting gas in this region, as inferred from spectral measurements by the Einstein SSS, is ~ 3 x 10^{-9} dyne cm^{-2}, placing it in approximate equilibrium with the cooler, denser, optically-emitting gas (Fesen and Kirshner 1980). Coupled with the general overlap between the regions of high X-ray surface brightness and the bright northern optical filaments, this suggests that the X-ray emitting gas may be interspersed among the sites of unstable radiative cooling which appear as optical filaments, and that both have arisen from the collision of the shock front with the molecular cloud.

The molecular cloud may affect the observed low-energy structure of IC 443 in a second way. As is visible in Figures 2 and 3, a lane of high optical extinction bisects IC 443 from northwest to southeast, extending a finger into the bright optical filaments. This lane demarcates another portion of the molecular cloud. The detection of shocked [H I] and a variety of molecular species with typical velocities around -30 km s^{-1} suggests that the front of the IC443 shell is colliding with the molecular cloud (see, e.g., Giovanelli and Haynes 1979; DeNoyer 1979). Although no general correlation between the X-ray surface brightness, as measured by the IPC, and the column density of the cloud, as inferred from the CO brightness temperature, is apparent, a correlation between column density and X-ray spectral hardness ratio

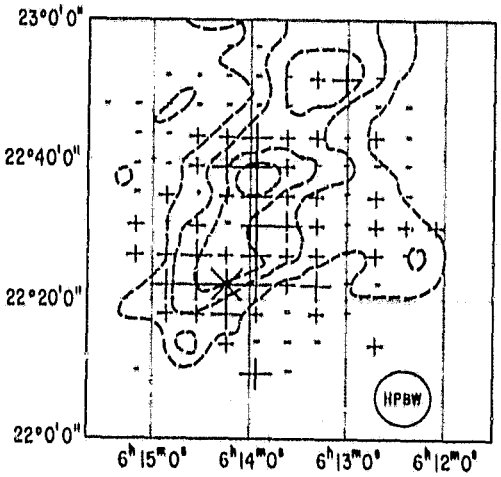

Figure 4: An IPC spectral hardness ratio map of IC 443, superposed on CO brightness temperature contours (from Cornett, Chin and Knapp 1977). Spectral hardness is defined as the ratio between 0.2-1.3 kev counts and 1.3-3.1 keV counts, with symbols of increasing prominence representing ratios of 0.6, 0.8, 1.0 and 1.2. Circle is HPBW of CO map.

(0.2-1.3 kev/1.3-3.1 kev) does exist. As seen in Figure 4, X-rays from regions coincident with the cloud are harder (average hardness ratio of ~ 0.8) than elsewhere in the remnant (average hardness ratio of ~ 0.6). To account for this increase of spectral hardness by absorption, a column density through the cloud of 2-4 x 10^{21} cm^{-2} is required (in addition to the column density to IC 443) if the characteristic temperature of IC 443 is uniform and within the range of 0.5-1.5 kev. This additional column density may be compared to the inferred average column density of H_2 through the cloud of 2 x 10^{21} cm^{-2} (i.e., 4 x 10^{21} cm^{-2} of [H I] - Cornett, Chin and Knapp 1977). It is thus probable that the cloud absorbs X-rays emitted by the interior of IC 443.

REFERENCES

Cornett, R.H., Chin, G., and Knapp, G.R. 1977, Astron. Ap., 54, pp. 889-894.

DeNoyer, L.K. 1979, Ap. J. (Letters), 228, pp. L41-L43.

Fesen, R.A., and Kirshner, R.P. 1980, Ap. J., 242, pp. 1023-1040.

Giovanelli, R., and Haynes, M.P. 1979, Ap. J., 230, pp. 404-414.

Petre, R., Canizares, C.R., Kriss, G.A., and Winkler, P.F. 1982a, Ap. J., 258, pp. 22-30.

Petre, R., Szymkowiak, A.E., Canizares, C.R., Seward, F.D., Willingale, R., Rolf, D., and Woods, N. 1982b, in preparation.

Scoville, N.Z., Irvine, W.M., Wannier, P.G., and Predmore, C.R. 1977, Ap. J., 216, pp. 320-328.

THE [AN]ISOTROPY OF THE X-RAY SKY

R.A. Shafer, NASA/Goddard Space Flight Center and Dept. of Physics and Astronomy, University of Maryland, U.S.A. (currently at Institute of Astronomy, Cambridge, U.K.)
A.C. Fabian, Institute of Astronomy, Cambridge, U.K.

1. Introduction

In this presentation we show how the study of the isotropy of the X-ray sky contributes to our understanding of the structure of the universe at moderate redshifts ($1 \lesssim z << z_{recombination}$). Actually, the anisotropy of the sky flux provides the information, much as the microwave sky anisotropy does for earlier epochs. [See reports in this volume.] Though we are currently unable to make measurements with the precision and small solid angles typically achieved in the microwave, comparatively crude limits from the X-ray fluctuations place limits on the largest scale structure of the universe. We first outline the measurements of the X-ray sky and its anisotropies made with the HEAO 1 A-2 experiment. Detailed presentations are found elsewhere [Shafer 1982; Marshall et al. 1980; Piccinotti et al. 1982; Iwan et al. 1982; Shafer et al. in prep.]. We then show how the anisotropies place limits on the origin of the X-ray sky and on any large scale structure of the universe, following the example of previous analyses which used earlier anisotropy estimates [see e.g. Fabian and Rees 1978; Rees 1980; Fabian 1981].

2. The X-ray Sky

In Figure 1 we present the extragalactic sky spectrum. Several properties of the X-ray portion of the spectrum are noteworthy:

(1) It is bright. A spectrum with slope -1 in Figure 1 has equal energy per decade; thus the energy density in 3-100 keV X-rays is second only to the density of the microwave region.

(2) It is easily detected and nearly isotropic. The region from about 3 keV to ~1 MeV is the only well studied portion of the sky spectrum other than the microwave background that is not dominated by a strong galactic component.

(3) It has a well determined, if not well understood, spectrum. In terms of accuracy and bandwidth the measurement of the X-ray spectrum surpasses even determinations of the microwave spectrum [de Zotti

PAGE 30 INTENTIONALLY BLANK

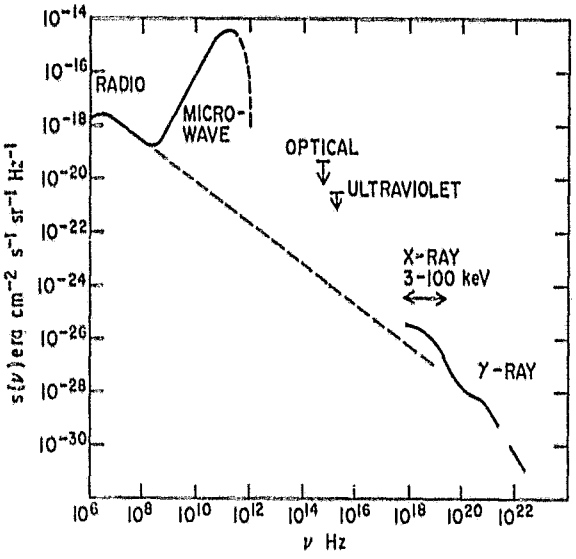

Figure 1. The Cosmic Extragalactic Spectrum. The light dashed line extends the radio discrete sources to higher energies assuming a 0.7 energy spectral index. [Radio and microwave: Longair 1978; Optical: Dube, Wickes and Wilkinson 1979; UV: Paresce, McKee and Bowyer 1980; X-ray: Marshall et al. 1980, Rothschild et al. 1983; γ-ray: Fichtel & Trombka 1981].

1982a]. The spectrum from 3 to 100 keV is well represented by a thin thermal bremsstrahlung model with a temperature of 40±5 keV [Marshall et al. 1980; Rothschild et al. 1983]. No population of sources with a single index power law spectra provides the right shape. A suitably constrained model of an evolving population with a sharp break in their spectral index is consistent with the 3-50 keV data [de Zotti et al. 1982b].

A variety of models have been presented to account for parts of the sky flux, but no coherent picture exists that satisfies all the observations. Particular models may be consistent with the data but all leave open questions or await particular observational confirmation. Known and possible fractions of the X-ray sky flux are:

(1) A galactic component. Because of the observed isotropy of the sky, any flux associated with the galactic disk can contribute no more than ~2-10% of the high galactic latitude flux, depending on the latitude of the observation [see e.g. Iwan et al. 1982]. In addition, known populations of galactic sources do not generally have the same spectrum as the sky.

(2) Well observed extragalactic sources. Based on the HEAO 1 A-2 all-sky survey the extragalactic sources resolved at high flux are predominantly either clusters of galaxies or active galactic nuclei (Seyferts, N galaxies, etc.) [Piccinotti et al. 1982]. The derived local luminosity function of these two populations can be used to estimate contributions to the total sky flux of about 4% and 18% respectively, assuming no significant evolution of the luminosity function. In addition, the low temperature thermal spectra of cluster sources [Mushotzky et al. 1978] and the power law spectra with a photon index near 1.7 typical of active galaxies do not correspond to the sky spectrum [Mushotzky et al. 1980; Rothschild et al. 1983]. In fact, no source or population has been observed to have the proper spectrum to provide the bulk of the sky emission.

(3) An evolving population of sources. This could be the evolution of

the above known populations or the introduction of a new population of sources. QSOs, which are undergoing apparent evolution at other wavelengths, have been shown to be strong emitters in the softer 0.5 to 3.5 keV band covered by the Einstein observatory [see e.g. Zamorani et al. 1981]. Unfortunately, there are too few high quality broad band X-ray spectra of QSOs to make an unambiguous estimate of their contribution at the higher energies typical of the bulk of the X-ray sky flux. Avni [1978] pointed out that active galaxies may make up the total sky flux if they undergo only moderate evolution, in comparison to the amount of evolution suggested for QSOs in the optical. However, the evolution must involve the spectral form of the objects as well as their luminosity function [e.g. Leiter and Boldt 1982]. Suggestions for new populations of X-ray sources have included hot gas associated with the initial generation of stars of young galaxies [Bookbinder et al. 1980] and primordial black holes [Carr 1980]. Though the proposed spectra are in accordance with the X-ray sky spectrum, there have been no identifications of these new objects with observed X-ray sources.

(3) A totally diffuse component, such as a hot intergalactic medium. This model has the correct spectral form, but there are possible difficulties providing the energy to heat the medium [Field and Perrenod 1977; Fabian 1981].

Though the exact origin of the sky flux is still an open question, we have a better understanding of the principal sources of the observed anisotropy. We classify the variations in the X-ray sky intensity as large angular scale anisotropies or as fluctuations (small scale variations).

The galaxy does not dominate the 2-10 keV sky flux, but the dominant large scale variation is associated with the galactic disk. An early model of this variation was the cosecant |b| law of an infinite plane of emission [Warwick, Pye and Fabian 1980]. Other studies have noted a longitudinal component associated with the galaxy [Protheroe, Wolfendale and Wdowczyk 1980; Iwan et al. 1982]. An expected large scale anisotropy, of smaller magnitude, is a cosine or dipole anisotropy. Such a signal is expected for the same reason as the dipole variation seen in the microwave sky, i.e. motion of the observer with respect to the rest frame of the emission, the Compton-Getting effect.

The dominant contribution to the small scale fluctuations is a continuation of known source populations to lower flux levels where sources are no longer individually detectable. The size and shape of the frequency distribution of the fluctuations is a function of the number of sources versus flux relation, N(S), at those fluxes. We can explain all the fluctuations in terms of the known populations, without evolution, and place an upper bound on the size of any other small scale variations, hereafter referred to as the excess variance. This bound constrains all other sources of anisotropy. Possible origins of additional variation would be an evolving or new population of sources, or a clumping of the sources that make up the background. At the largest angular scales source clumping indicates large scale structure

in the universe, such as a global perturbation in the density $\delta\rho$. An upper bound on the excess variance limits the allowed strength of such structure, $\delta\rho/\rho$, with no assumption about the origins of the X-ray sky flux other than presuming that variations in the X-ray volume emissivity are proportional to $\delta\rho$. (For general reviews of the X-ray sky see e.g. Boldt [1981], Fabian [1981].)

3. The Data

Our results are based on measurements taken with a xenon proportional counter, one module of the A-2 experiment on the HEAO 1 satellite [Rothschild et al. 1979], taken during an all-sky survey. For the X-ray sky spectrum, 90% of the counts in this detector originate in the 2.5-13.3 keV band. We measure flux, S, in units of counts s^{-1} cm^{-2}. For typical extragalactic spectra 1 count s^{-1} cm^{-2} is equivalent to 1.35×10^{-8} ergs s^{-1} cm^{-2} (2-10 keV). The all-sky flux, S_{as}, is 58 counts s^{-1} cm^{-2}. The measured count rate depends on detector area, collimator solid angle, and integration time. For our measurements the mean sky intensity, I_{sky}, is 17.06 counts exp^{-1} (one exposure is 1.28 s). The mean count rate of the internal, non-X-ray, background is 3.5 counts exp^{-1}. The average uncertainty due to counting statistics was 0.23 counts exp^{-1}. The angular size of the measurements is fairly large, over 100 square degrees, but much of this area contributes little to the total count rate. 90% of the total comes from a rectangle of $11.2^{\circ}\times4.4^{\circ}$, covering 49 square degrees. The central area of ~26 square degrees contributes 71% of the sky intensity but 90% of any excess variance in the intensity.

The fluctuation data were restricted to high galactic latitudes, $|b|>20^{\circ}$, and free from contamination by X-ray sources in the Magellanic Clouds and bright high latitude galactic sources. When looking for large scale structure, we included data down to latitudes of 10°, excluding all contamination from any resolved source cataloged in the complete all-sky sample of Piccinotti et al.[1982].

The A-2 detectors had several unique features for the continuous monitoring of internal background and determining the X-ray sky flux. The performance of the detectors, as monitored by repeat scans of the same area of the sky six months apart, was very stable. The internal background was also very stable. After selection of data to avoid noisy periods, the variation in the background was roughly 0.05 counts exp^{-1}, corresponding to a sigma 1.3% of the non-X-ray count rate and only 0.25% of the total intensity.

4. Large scale variations: Galactic and Dipole anisotropies

Using a similar set of HEAO 1 A-2 data, Iwan et al.[1982] showed that there was a variation associated with galactic longitude in addition to the latitude variation. Following that paper we fit the galactic component with a disk of finite radius and an exponential scale height. These parameters are strongly correlated and their upper bounds

poorly determined. The best fit radius was 1.8 R_{gc}, where R_{gc} is the distance from the sun to the galactic center, roughly 10 kpc. The best fit value for the scale height was 0.4 R_{gc}, with the 90% lower limit of 0.1R_{gc}, corresponding to 1 kpc, a scale typically larger than most galactic X-ray source populations. A discussion of this model and its implications is given in Iwan et al. [1982].

After removal of the best fit galactic model, we fit a dipole model, $\delta I = I_{CG} \cos \theta$, where θ is the angle between the observation and the signal maximum. The addition of this new model to the fit produced a drop in χ^2 significant at the 95% level. The strength of the signal, I_{CG}, is 0.09±0.03 counts exp^{-1}, about 0.5% of the sky intensity. The best fit direction in galactic coordinates, (ℓ,b), is (282°,+30°). However the 90% confidence region for the direction is very large, covering about one eighth of the total sky. A result of similar direction, magnitude, precision, and confidence was found by Protheroe, Wolfendale and Wdoczyk [1980] using UHURU data.

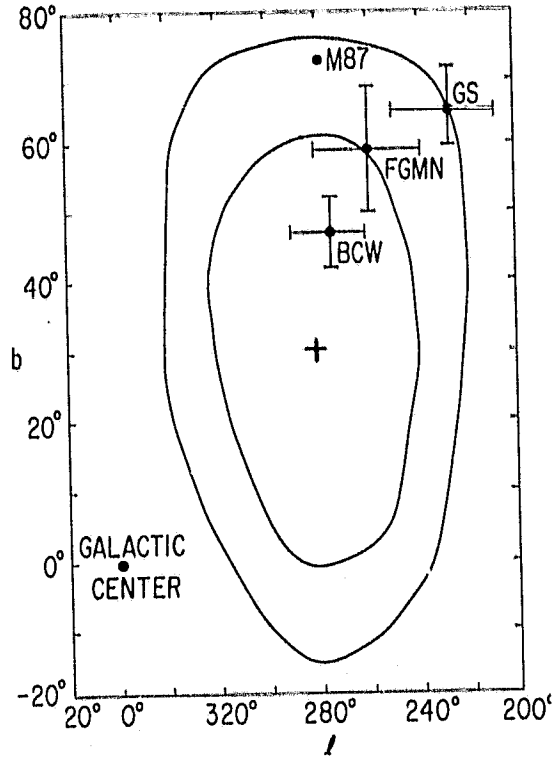

Figure 2. Position of Dipole Maximum. Contours show 70% and 90% confidence regions. The center + marks the best fit position. Also shown are the one-sigma error bars for measurements of the dipole maximum in the microwave. [BCW: Boughn, Cheng & Wilkinson 1981; FGMN: Fabbri, Guidi, Melchiorri and Natale 1980; GS: Gorenstein and Smoot 1981.]

One possible interpretation of this statistically marginal result is in terms of the Compton-Getting effect, where the size of the dipole signal is related to the observer's velocity by

$$I_{CG} = \bar{I} \, (2+\Gamma) \, v/c. \qquad [1]$$

Γ is the photon index of the sky flux, ~1.4 for the band we are interested in. The derived value for the velocity, 475±165 km s^{-1}, and

the direction are consistent with observations of the dipole signal in the microwave sky. The microwave directions in the literature are shown in Figure 2 along with the X-ray confidence regions. A synthesis performed by Wilkinson at this symposium of the different experimental results gave a best fit direction of $(265^{o},+50^{o})$ and a velocity of 372 ± 25 km s^{-1}. The origins of the Compton-Getting velocity may be responsible for an additional component of the observed X-ray dipole signal. If the velocity observed in the microwave is the integral of the acceleration caused by a large scale overdensity ("lump") at the same redshifts range at which the X-ray sky emission originates, then the lump should produce an excess in the X-ray emissivity, producing an enhancement in the direction of the lump in addition to the Compton-Getting velocity signal. Comparisons of the X-ray and microwave large-scale anisotropies help to decouple the two effects of such a lump, providing constraints on the lump's properties. [see e.g. Warwick, Pye and Fabian 1980; Fabian 1981].

The total dipole signal may be due to variations other than the Compton-Getting effect. The form of the underlying structure may not be a pure dipole. For instance, there may be second order anisotropies associated with the galaxy but not included in the finite disk model. Also, it is intriguing that the contour for the direction of the dipole maximum includes a large fraction of the local supercluster, which could provide a large scale enhancement to the sky flux. The best fit value of I_{CG} corresponds to a maximum surface brightness of 0.02 counts s^{-1} cm^{-2} sr^{-1}. The volume emissivity and total luminosity of the local supercluster required to dominate the "dipole" signal are dependent on geometry. Assuming a disk of emission centered on the dipole maximum with a radius of 4 Mpc, an estimate of the total luminosity is 2×10^{42} erg s^{-1} (H_{o} = 50). Previous attempts to correlate X-ray surface brightness with the local supercluster have yielded only upper limits larger than the above estimates. [see e.g. Schwartz 1980]. To test if the local supercluster is in part responsible for the fit dipole signal requires direct testing of models for the supercluster, a project now in progress. The tidal "12 hour" signal reported by Warwick, Pye and Fabian [1980] in the Ariel V data was not observed in the A-2 data.

5. Small Scale Anisotropies: The Fluctuations

Point sources have an impact on measurements of the sky flux even if the sources are too numerous to be individually resolved. The actual number of sources, and hence their total intensity, varies from one part of the sky to another. The process of extracting information about the sources from the size and shape of the intensity distributions was pioneered by radio astronomers [Scheuer 1957; Condon 1974; see e.g. Condon and Dressel 1978]. Given a model for the differential number of sources as a function of flux, N(S) dS, the distribution of intensities, $P_{I-\bar{I}}(I)$ dI, can be predicted, assuming the distribution of sources is completely random and unclumped. Standard statistical tools are used to evaluate the N(S) models by comparing the predicted distributions to observations, extending our knowledge of the X-ray

source counts beyond what was directly accessible from resolved sources [Fabian 1975; Schwartz 1976; Pye and Warwick 1976].

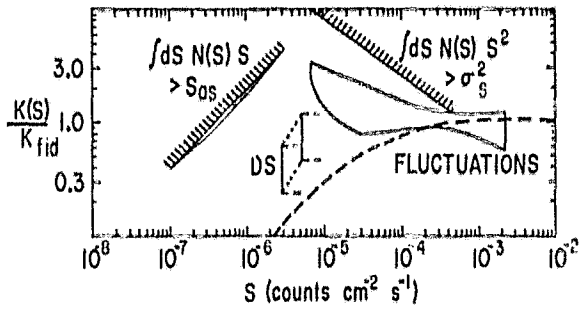

Figure 3. Number of Sources Versus Flux Derived from the Fluctuations. The plotted quantity is the ratio of the number to that expected for a fiducial Euclidean model, where $N \propto S^{-5/2}$. See text for details.

In Figure 3 we present the results of such model fitting using the HEAO 1 A-2 data. We restricted our model to a single power law form,

$$N(S)\, dS = 4\pi\, K\, S^{-\gamma}\, dS\ , \qquad [2]$$

with a sharp cutoff imposed at the low flux where the intensity contributed by the sources equals the total sky flux:

$$\int dS\ N(S)\ S = S_{as}\ . \qquad [3]$$

A population of sources distributed randomly through Euclidean space will follow a power law model with $\gamma = 5/2$. We compare an N(S) relation to the Euclidean form by defining a function K(S)

$$N(S) \equiv 4\pi\ K(S)\ S^{-5/2}. \qquad [4]$$

Figure 3 plots K(S) with respect to K_{fid}, the K value for the best fit Euclidean model, 1.48×10^{-3} (counts s^{-1} cm^{-2})$^{1.5}$. Other Euclidean models would appear on Figure 3 as horizontal lines, K(S) constant. The trumpet-shaped region on the right shows the behavior of power law models acceptable at the 90% level. The hatched line at the far left is where the power law models must be terminated to avoid exceeding the total sky flux (equation [3]). With our data, an acceptable power law model that is truncated between the hatched line and the left hand edge of the trumpet shaped region is statistically indistinguishable from the model as continued to the hatched line. The right hand edge shows the limits of the HEAO 1 resolved source counts.

The greatest constraint placed by the fluctuations is on sources roughly an order of magnitude in flux below resolved sources. However care is required in interpreting the limits on N(S). The formal validity of the confidence region rests on the assumption that the actual N(S) is well modelled by a single power law continuing without change of index past the lower limits of the region. More complicated models that do not lie wholly within the indicated region may be acceptable, e.g. the dashed line of Figure 3. This line is a schematic representation of the N(S) behavior of sources observed directly at higher fluxes and extrapolated without evolution to the lower values of

S using the appropriate luminosity functions.

To assess the degree of source evolution at low fluxes, direct measuments of N(S) would be the easiest to interpret. The deep surveys performed with the Einstein observatory [e.g. Giacconi et al. 1979] provide such information. However information from the deep survey, indicated by the two bars labeled DS in Figure 3, also have problems of interpretation. One difficulty is in transforming source fluxes from the Einstein 1-3 keV band to the higher energy band measured in the A-2 data without good spectral information. The upper-right bar of the pair uses the published presumption that the sources have a 1.4 index power law photon spectrum, typical of the unresolved sky flux in the 2-10 keV band. The lower-left bar instead assumes that the deep survey sources have the 1.7 index spectra characteristic of active galactic nuclei. Both bars assume that N(S) is Euclidean at the deep survey flux limit. If γ were nearer that of the unevolved population's models at that flux, $\gamma \sim 1.8$, or if the sources were strongly evolving so that γ were near 3, the bars would be adjusted to 50%-130% of their indicated value. Conclusions drawn from the deep survey results must explictly consider the impact of these assumptions. Results from the Einstein medium survey [see e.g. Maccacaro et al. 1982] show source evolution less indirectly.

6. Excess Variance

The fluctuations can be totally described by models of non-evolving sources, such as the dashed line in Figure 3. The 90% upper bound to any additional variance, added as a pure Gaussian, is $\sigma^2_I \leq 0.057$ (counts $\exp^{-1})^2$. If we assume that the unevolved populations account for 20% of the sky intensity then σ_I is $\leq$1.7% of the remaining intensity. Any other source of variation is constrained by this limit.

Any evolving populations's distribution, $N_{ev}(S)$, is a source of fluctuations. It must satisfy the integral constraint

$$\sigma^2_S = \int dS\ S^2\ N_{ev}(S)\ . \qquad [5]$$

σ^2_S is a measure of the excess variance that is independent of the measurement solid angle, $\sigma^2_S \leq 7\times10^{-4}$ (counts s^{-1} $cm^{-2})^2$. The impact of this limit depends on the particular form of $N_{ev}(S)$ but if the evolved sources are to make up the remainder of the sky flux we place a lower limit on the number of sources at 75 per square degree and an upper limit on their mean flux at 1.5×10^{-5} counts s^{-1} cm^{-2} (2.0×10^{-13} erg s^{-1} cm^{-2}). If we assume that $N_{ev}(S)$ is of the form $4\pi\ K_{ev}\ S^{-3}$ we can set a limit $K \leq 1.7\times10^{-5}$ (counts s^{-1} $cm^{-2})^2$, indicated by the right-hand hatched line in Figure 3. A wide latitude for the behavior of $N_{ev}(S)$ is allowed.

These limits all assume that the sources that make up the background are not clustered, that is, their distribution among the measurements is Poisson. We can estimate that the total allowed

variation on a scale of 26 square degrees, roughly the size of a Schmidt survey plate, is 2.3%. If QSOs contribute all of the remaining sky flux, then this limit means that the total $(\delta N/\bar{N})_{QSO} \lesssim 0.023$, where $\bar{N}$ is the mean number of QSOs on a scale of 26 square degrees, and δN is the total variation including Poisson statistics and clumping. If we assume the number of QSOs is ~200 per square degree in order to estimate the Poisson noise portion, the additional variation due to clumping can be at most 1.9%. If QSOs are observed to have clustering with a larger value of δN on these scales, then the excess variance places an upper bound on their contribution to the total sky flux.

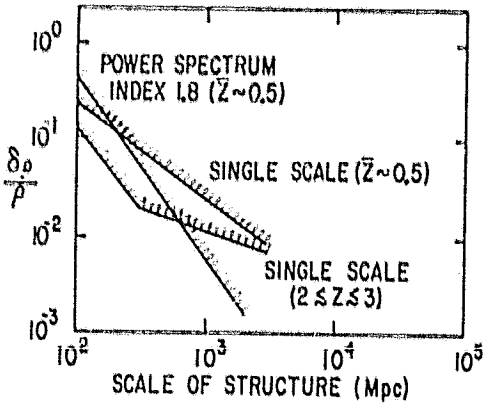

Figure 4. Preliminary upper bounds on magnitude of large scale structure from limits of X-ray excess variance.

Figure 4 shows estimates of the limits on the large scale structure of the universe placed by a previous upper bound on the excess variance. The three curves illustrate the dependence of the limits on models of the structure as well as on the origins of the X-ray sky. Two of the curves compare the case for an unevolved origin of the sky flux, $\bar{z}$~0.5, and the density variation restricted to a single scale or defined by a power spectrum with index 1.8, typical of the inferred distribution at smaller scales [see e.g. Peebles 1980]. The third curve is for a single scale of variation where the sky flux is dominated by an evolved component with $2 \lesssim z \lesssim 3$.

7. Conclusions

All small scale fluctuations are consistent with what we expect from known, unevolved populations of sources resolved by HEAO 1. The large scale variation, dominated by a galactic anisotropy, also admits a dipole signal which may be interpreted as a Compton-Getting dipole signal consistent with the microwave results, although other interpretations are possible. The bound on any excess variance places limits on structures at moderate redshift and of large scale otherwise not easily accessible.

We would like to thank our colleagues at GSFC, particularly C.M. Urry, for their contributions and critical advice on this presentation. ACF aknowledges the financial support of the Royal Society of London.

References

Avni, Y., 1978, Astron. Astrophys., 63, L13.
Boldt, Elihu, 1981, Comments Astrophys., 9, 97.
Bookbinder, J., L.L.Cowie, J.H.Krolik, J.P.Ostriker & M.J.Rees, 1980, Ap.J., 237, 647.
Boughn, S.P., E.S.Cheng & D.T.Wilkinson, 1981, Ap.J.(Lett.), 243, L113.
Carr, B.J., 1980, Nature, 284, 326.
Condon, J.J., 1974, Ap.J., 188, 279.
Condon, J.J., & L.L.Dressel, 1978, Ap.J., 222, 745.
de Zotti, G., 1982a, Acta Cosmol., 11, 65.
de Zotti, G., E.A.Boldt, A.Cavaliere, L.Danese, A.Franceschini, F.E.Marshall, J.H.Swank & A.E.Szymkowiak, 1982, Ap.J., 253, 47.
Dube, R.R., W.C.Wickes & D.T.Wilkinson, 1979, Ap.J., 232, 333.
Fabbri, R., I.Guidi, F.Melchiorri & V.Natale, 1980, Phys.Rev.Lett., 44, 1563. (Erratum in 45, 401).
Fabian, A.C., 1975, M.N.R.A.S., 172, 149.
Fabian, A.C., & M.J.Rees, 1978, M.N.R.A.S., 185, 109.
Fabian, A.C., 1981, in Ramaty and Jones (eds.), 10th Texas Symposium on Relativistic Astrophysics, Ann.N.Y.Acad.,Sci., 375, 235.
Fichtel, C.E. & J.I.Trombka, 1981, Gamma Ray Astrophysics, NASA SP-453, (Government Printing Office:Washington).
Field, G.B., & S.C.Perrenod, 1977, Ap.J., 215, 717.
Giacconi, R., J.Bechtold, B.Branduardi, W.Forman, J.P.Henry, C.Jones, E.Kellogg, H.van der Laan, W.Liller, H.Marshall, S.S.Murray, J.Pye, E.Schreier, W.L.W.Sargent, F.Seward & H.Tananbaum, 1979, Ap.J.(Lett.), 234, L1.
Gorenstein, M.V., & G.F.Smoot, 1981, Ap.J., 244, 361.
Iwan, D., F.E.Marshall, E.A.Boldt, R.F.Mushotzky, R.A.Shafer & A.Stottlemyer, 1982, Ap.J., 260, 111.
Leiter, D. & E.Boldt, 1982, Ap.J., 260, 1.
Longair, M.S., 1978, in Gunn, Longair & Rees Observational Cosmology, (Geneva Observatory:Sauverny, Switzerland).
Maccacaro, T., Y.Avni, I.M.Gioia, P.Giommi, J.Liebert, J.Stocke, J.Danziger, 1982, Ap.J., subm.
Marshall, F.E., E.A.Boldt, S.S.Holt, R.Miller, R.F.Mushotzky, L.A.Rose, R.Rothschild & P.Serlemitsos, 1980, Ap.J., 235, 4.
Mushotzky, R.F., P.J.Serlemitsos, B.W.Smith, E.A.Boldt & S.S.Holt, 1978, Ap.J., 194, 1.
Mushotzky, R.F., F.E.Marshall, E.A.Boldt, S.S.Holt & P.J.Serlemitsos, 1980, Ap.J., 235, 377.
Paresce, F., C.F.McKee & S.Bowyer, 1980, Ap.J., 240, 387.
Piccinotti, G., R.F.Mushotzky, E.A.Boldt, S.S.Holt, F.E.Marshall, P.J.Serlemitsos & R.A.Shafer, 1982, Ap.J., 253, 485.
Peebles, P.J.E., 1980, The Large-Scale Structure of the Universe, (Princeton University Press:Princeton).
Protheroe, R.J., A.W.Wolfendale & J.Wdowczyk, 1980, M.N.R.A.S., 192, 445.
Pye, J.P. & R.S.Warwick, 1979, M.N.R.A.S., 187, 905.
Rees, M.J., 1980, in Abell and Peebles (eds.), Objects at High Redshifts, I.A.U. Symp. 92, 209, (D. Reidel:Dordrecht).

Rothschild, R., E.Boldt, S.Holt, P.Serlemitsos, G.Garmire, P.Agrawal, G.Riegler, S.Bowyer & M.Lampton, 1979, Space Sci.Inst., 4, 269.
Rothschild, R.E., R.F.Mushotzky, W.A.Baity, D.E.Gruber & J.L.Matteson, 1983, Ap.J., submit.
Scheuer, P.A.G. 1957, Proc.Camb.Phil.Soc., 53, 764.
Schwartz, D.A., S.S.Murray, H.Gursky, 1976, Ap.J., 204, 215.
Schwartz, D.A., 1980, Physica Scripta, 21, 644.
Shafer, R.A., 1982, Ph.D. dissertation, University of Maryland.
Shafer, R.A., et al., 1983, in prep.
Warwick, R.S., J.P.Pye & A.C.Fabian, 1980. M.N.R.A.S., 190, 243.
Zamorani, G., J.P.Henry, T.Maccacaro, H.Tananbaum, A.Soltan, Y.Avni, J.Lieber, J.Stocke, P.A.Strittmatter, R.J.Weymann, M.G.Smith, J.J.Condon, 1981, Ap.J., 245, 357.

X-RAY OBSERVATIONS OF ACTIVE GALACTIC NUCLEI

C. Megan Urry[1],

Richard F. Mushotzky, Allyn F. Tennant[2],

Elihu A. Boldt, Stephen S. Holt

NASA/Goddard Space Flight Center, Greenbelt, MD, USA

ABSTRACT

HEAO 1 A2 and Einstein SSS spectral observations of Seyfert galaxies and BL Lac objects suggest that in both cases, the X-ray emission is due to relativistic particles. The five BL Lac objects have very soft spectra and at higher energies (above 10 keV) may have hard tails. Combining our X-ray data with radio, infrared, optical, and ultraviolet observations, we can fit the BL Lac spectra with the familiar synchrotron self-Compton model if we allow for relativistic beaming (Urry and Mushotzky 1982, Urry et al. 1982). We show that Doppler beaming of an underlying (Seyfert-like) source population flattens the observed luminosity function, and we emphasize that the relative numbers of BL Lacs and quasars in given spectral intervals are strong functions of selection effects, the degree of Doppler beaming,

[1]also Johns Hopkins University, Baltimore, MD, USA
[2]also University of Maryland, College Park, MD, USA

and the form of the intrinsic luminosity function.

The twenty-eight X-ray spectra of Seyfert galaxies are remarkably homogeneous: all are well-fit by power laws with mean energy spectral index $\alpha = 0.65 \pm 0.13$, where the latter number indicates the dispersion (Mushotzky et al. 1980, Mushotzky 1982). This power law, taken with the IR-optical-UV emission, suggests that Compton scattering is the dominant X-ray production mechanism. No changes in spectral form are seen on short ($10-10^4$ s) or long (0.5-1.5 yr) timescales in either the A2 (2-40 keV) or SSS (0.5-3.5 keV) data even when the intensity of the source changes. With one major exception (NGC 6814), no variability with $\Delta I/I > 0.1$ is seen for timescales of 5 seconds to 6 hours (Tennant and Mushotzky 1982). For 6 month timescales, at most one third of the galaxies are variable in intensity, and these tend to be the lower luminosity objects.

REFERENCES

Mushotzky, R. F. 1982, Ap. J., 256, 92.

Mushotzky, R. F., Marshall, F. E., Boldt, E. A., Holt, S. S., and Serlemitsos, P. J. 1980, Ap. J., 235, 377.

Tennant, A. F. and Mushotzky, R. F. 1982, Ap. J., 264.

Urry, C. M. and Mushotzky, R. F. 1982, Ap. J., 253, 38.

Urry, C. M., Mushotzky, R. F., Kondo, Y., Hackney, K. R. H., and Hackney, R. L. 1982, Ap. J., 261, 12.